NONLINEAR STABILITY ANALYSIS OF ACTIVE MAGNETIC BEARINGS

Norbert Steinschaden and Helmut Springer
Institute for Machine Dynamics and Measurements,
Vienna University of Technology,
Wiedner Hauptstraße 8-10 / E303, A-1040 Vienna, Austria.

ABSTRACT

In order to get a better understanding of the dynamics of active magnetic bearing (AMB) systems under extreme operating conditions a nonlinear model for a radial AMB system is investigated. Instead of the common way of linearizing the magnetic forces at the center position of the rotor with respect to rotor displacement and coil current, the fully nonlinear force to displacement and force to current characteristics are used. The nonlinear model employed in this investigation is an advanced version of a simple nonlinear model, which has already been published and discussed in [Steinschaden, Springer, 1999]. Magnetic saturation effects, saturation of the amplifier and limitations of the control currents are additional nonlinear components modeled in this work.

The AMB system is excited by unbalance forces of the rotor. Especially for the case of large rotor eccentricities, causing large rotor displacements, the behaviour of the system is discussed. A path-following analysis of the equations of motion shows that for some combinations of parameters well-known nonlinear phenomena may occur.

INTRODUCTION

AMBs represent modern mechatronical systems. The avoidance of any lubrication systems and lubricants, the absence of material wear and almost no friction losses, as a consequence of no mechanical or fluidic contact between the rotor and the stator, are significant advantages resulting in high life time and low maintenance requirements, see [Schweitzer, et al., 1993]. If magnetic bearings are used, no additional equipment will be needed for diagnosis and permanent monitoring tasks during machine operation. Stiffness, damping and force characteristics of the bearing can be adapted to actual machine operating conditions by adaptive control strategies easily implemented into the feedback control device, see [Lang, et al., 1995]. As the area of industrial applications of AMB systems grows, there is a growing demand of highly reliable systems at any operating conditions. This requires a deep and complete understanding of the dynamics of rotor-AMB systems.

For a rigid rotor supported by two lubricated journal bearings Moser has investigated the nonlinear stability and bifurcation behaviour in terms of three important dimensionless bifurcation parameters, [Moser, 1993]. They correspond to the rotor speed, the static load and the unbalance eccentricity of the rotor. For magnetic bearings, there are only a few papers available that partially deal with the problem of nonlinear modeling, stability and bifurcation. Hebbale investigated a four-magnet AMB system with linear state variable control and pole placement design, [Hebbale, 1985, Hebbale, Taylor, 1986]. A two degrees of freedom single-mass rotor with nonlaminated (solid) ferromagnetic flux paths was considered which generates speed dependent eddy current effects due to rotation of the rotor. By applying the center manifold theory, see [Troger, Steindl, 1991], a subcritical Hopf bifurcation was detected in terms of the rotor speed being the bifurcation parameter. Furthermore, in [Hebbale, 1985, Hebbale, Taylor, 1986] the influence of rotor unbalance on the stability was investigated by numerical simulation studies.

Mohamed and Emad investigated a rigid rotor in two radial AMBs with a linear state variable voltage controller, [Mohamed, Emad, 1993]. Nonlinear force to magnetic flux relationships were considered along with speed dependent gyroscopic effects of the rotor. A subcritical Hopf bifurcation was found for a static equilibrium state in terms of the rotor speed being the distinguished bifurcation parameter.

Wang et al. investigated a single-mass rotor (with and without unbalance) supported by an AMB with linear voltage PD-controller, [Wang, et al., 1994]. They considered nonlinear force to air gap and nonlinear force to coil current characteristics. Applying the center manifold theory, bifurcations were found in terms of the controller feedback gain parameters.

Ecker, Knight and Virgin found pitchfork and torus bifurcations for the vibrational amplitudes of an AMB-supported single-mass rotor with unbalance excitation in terms of the rotor speed as the distinguished bifurcation parameter, [Ecker, et al., 1997, Knight, Ecker, 1996, Virgin, et al., 1994]. Since they used flux control with a linear feedback law, the only nonlinearities were conservative cross coupling forces acting between two pairs of orthogonal oriented electromagnets, see [Knight, et al., 1993, Knight, et al., 1992].

Chinta et al. investigated the effects of cross-coupling forces using current control, where the nonlinear force to displacement and the nonlinear force to coil current characteristics are additionally active, [Chinta, et al., 1996]. Again an AMB system with a single-mass rotor excited by unbalance forces is considered. They used the tool of numerical simulation method. Quasiperiodic and period-2 solutions for the rotor vibration were found.

Beside the above discussed references several authors applied the classical methods of harmonic balance, describing function and perturbation theory to autonomous or non-autonomous AMB systems, see [Hoffmann, et al., 1997, Knight, et al., 1993, Nataraj, 1995, Sinha, 1990]. Moreover, stable limit cycles as response to speed synchronous unbalance excitation were found by the tool of numerical simulation, see [Haferl, Springer, 1991, Jeong, et al., 1994, Knight, Ecker, 1996, Knight, et al., 1993, Satoh, et al., 1990, Springer, et al., 1990].

This paper discusses the dynamic characteristics of an AMB-supported single-mass rotor with speed synchronous unbalance excitation. The mathematical model includes nonlinear force to displacement and force to coil current relationships. Nonlinear saturation effects of the magnetic materials as well as limitations, of the power amplifier and of the control current are considered in the present model. Effects of coil inductance combined with an underlying current controller are included as well.

AMB SYSTEM MODEL

Magnetic Force Model

The calculation of the magnetic forces generated by AMB-actuators is based on the commonly used one-dimensional model for the magnetic flux, see [Schweitzer, et al., 1993].

Leakage and fringing effects, are neglected. The permeability within the iron paths is considered to be finite and constant. Thus, the mathematical formulation of the magnetic force of one radial actuator can be presented as

$$f = k\frac{i^2}{4g^2\left(1+\frac{\mathcal{R}_{m1}}{\mathcal{R}_g}+\frac{\mathcal{R}_{m2}}{\mathcal{R}_g}\right)^2}, \tag{1}$$

where k is a constant value depending on the actuator properties, i is the coil current of the actuator and g is the radial air gap length between rotor and stator. $\mathcal{R}_g$ is the reluctance of the air gap and $\mathcal{R}_{mi}$ is the reluctance of an iron path i, which can be written as

$$\mathcal{R}_g = \frac{2g}{\mu_0 A_g}, \qquad \mathcal{R}_{mi} = \frac{l_{mi}}{\mu_0 \mu_{r,mi} A_{mi}}, \tag{2}$$

respectively, where μ_0 is the permeability of air, A_g is the cross section area of the air gap, l_{mi} is the length, $\mu_{r,mi}$ is the relative permeability and A_{mi} is the cross section area of iron path i.

Magnetic saturation effects within the iron paths are modeled by an approximation of the anhysteretic curve of the magnetic materials. Hysteresis effects are not considered in this investigation. Therefore, there is a definite relationship between magnetic flux density and magnetic field strength. The relative permeability of a magnetic material is a function of the magnetic flux density and is calculated from the empirical relation

$$\mu_{r,mi} = \frac{1-\mu_{r,mi,0}}{\pi}\arctan\left(K_{M,mi}\frac{|B_{mi}|-B_{mi,max}}{B_{mi,max}}\right)+\frac{1+\mu_{r,mi,0}}{2}, \tag{3}$$

where $\mu_{r,mi,0}$ is the relative permeability well below the saturation value $B_{mi,max}$, B_{mi} is the actual magnetic flux density and $K_{M,mi}$ is a shaping factor of the anhysteretic curve.

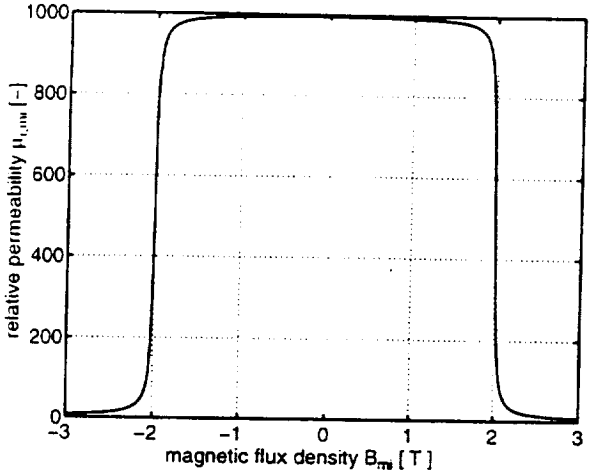

Figure 1: Relative permeability as a function of the magnetic flux density for the parameter values $\mu_{r,mi,0} = 1000$. $K_{M,mi} = 100$ and $B_{mi,max} = 2.0$T.

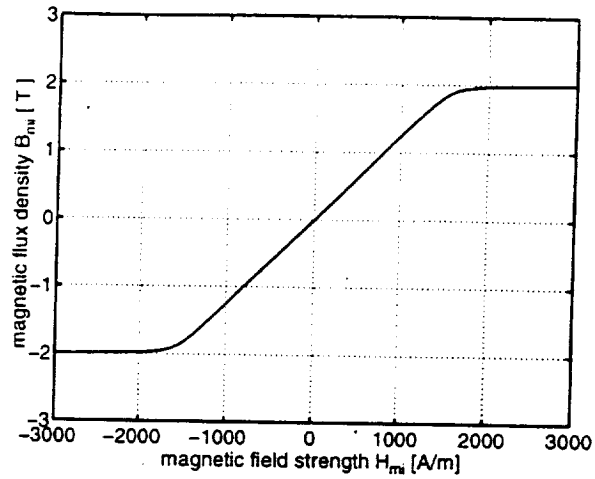

Figure 2: B-H curve for the parameter values $\mu_{r,mi,0} = 1000$, $K_{M,mi} = 100$ and $B_{mi,max} = 2.0$T.

Figure 1 shows the calculated relative permeability $\mu_{r,mi}$ as a function of the magnetic flux density B_{mi}. The corresponding approximation for the anhysteretic curve is shown in Fig. 2.

There is no specific parameter which determines the slope of the B-H curve above the saturation value. Instead, the slope is specified by the choice of the shaping factor $K_{M,mi}$. Equ. 3 allows a qualitatively good approximation within the range of interest of the magnetic flux density. It should be mentioned that this formulation should not be used in the case of very high values of the magnetic flux density far above the saturation value. However, such high values of magnetization are not achieved in common magnetic bearing systems.

The relatively simple structure of this mathematical formulation of the magnetic saturation characteristic is very useful for a successful application of the employed numerical solution method which allows a calculation of stable and unstable periodic solutions. See the section entitled 'Numerical Solution Methods.'

Magnetic Bearing Model

Figure 3 shows a schematic diagram of the axial view of an active magnetic bearing. The shaft is plotted in the center position ($x = 0$, $y = 0$, $g = g_0$). The magnetic bearing considered consists of two pairs of orthogonally oriented electromagnets. The magnet pairs are controlled independently. Any coupling effects between the directions x and y are neglected.

For each magnet pair one collocated displacement sensor measures the rotor position in the $x-$

and $y-$direction, respectively. The displacement signal is the input for the PID-current controller where the integral feedback gain eliminates steady state deviations from the center position of the rotor. According to the output of the controller, the amplifier supplies the voltage to produce the appropriate magnetic force in the actuator.

In order to achieve a stable damped system, a bias current, i_b, which has a static, predefined value, is supplied in each actuator and a control current, which corresponds to the controller output, is superimposed. It is very common to apply a so-called 'differential control', which means that one magnetic actuator input consists of the bias current plus the control current, while the input of the opposite actuator consists of the bias current minus the control current. Thus, the coil currents calculated by the controller for the actuators acting in $x-$ and $y-$directions, respectively, are given by

$$\begin{aligned} i_{C,x,+} &= i_b - G_P x - G_D \dot{x} - G_I \int_0^t x dt \\ i_{C,x,-} &= i_b + G_P x + G_D \dot{x} + G_I \int_0^t x dt \\ i_{C,y,+} &= i_b - G_P y - G_D \dot{y} - G_I \int_0^t y dt \\ i_{C,y,-} &= i_b + G_P y + G_D \dot{y} + G_I \int_0^t y dt, \end{aligned} \tag{4}$$

where G_P is the proportional feedback gain, G_D is the differential feedback gain and G_I is the integral feedback gain. The subscripts '+' and '-' identify the actuators located at the positive and negative axes, respectively (see Figure 3). In the special case, when the bearing does not carry a steady lateral load, the bias currents i_b will be equal in all actuators, which is assumed in the following.

This investigation includes the effects of coil inductance and requires an additional state variable for each magnetic flux. As a consequence of inductance the coil current does not instantanously follow the voltage applied by the power amplifier. Instead, the voltage drop u in each actuator coil has to be calculated from

$$u = Ri + N\dot{\Phi}, \tag{5}$$

where R is the electric resistance of the coil, i is the coil current, N is the number of coil turns and Φ is the magnetic flux of the actuator. In order to achieve a better dynamic behaviour of the magnetic bearing an underlying current controller is implemented. For that task a simple P-controller is employed. As a result the applied voltage is then given by

$$u = Ri_b + RG_{P,I}\left(i_b \mp i_c - i\right), \tag{6}$$

where $G_{P,I}$ is the proportional feedback gain of the underlying current controller, i_c is the control current calculated by the main PID-controller and i is the actual coil current.

Any power amplifier has an upper and a lower limit for the voltage which can be applied to the electromagnet. If the voltage determined by the underlying current controller exceeds the limited

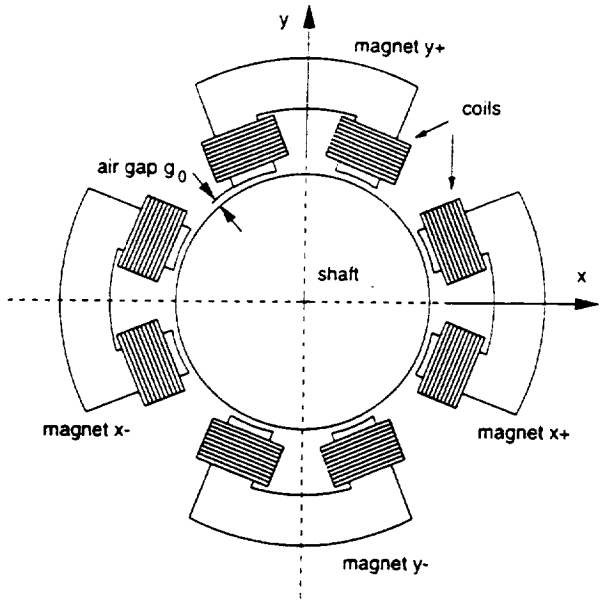

Figure 3: Schematic diagram of an 8-pole active magnetic bearing with the shaft in center position.

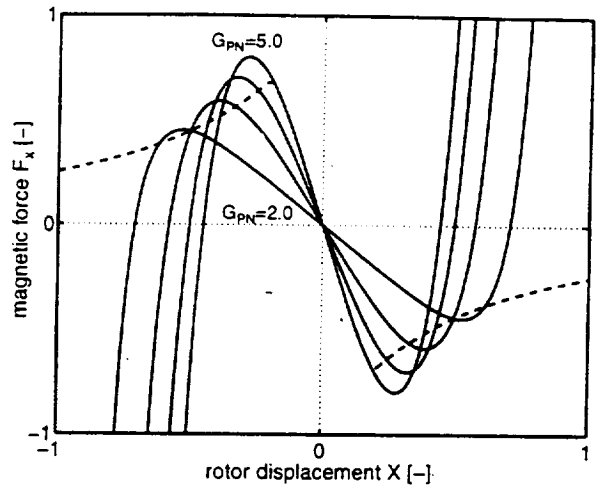

Figure 4: Nonlinear magnetic force exerted on the rotor for the quasistatic case. The proportional feedback $G_{P,V}$ is varied from 2.0 to 5.0.

range of voltage, the required voltage cannot be fully supplied. This results in a reduced slew rate of the coil currents and consequently of the magnetic forces. The saturation effect of the amplifier may cause poor dynamical behaviour of the magnetic bearing. It can be modeled by the empirical equation

$$\begin{aligned} u_a = u_n \;+\; & \left[\frac{1}{2} + \frac{1}{\pi}\arctan\left(K_U \frac{u_n - u_{max}}{u_{max}}\right)\right](u_{max} - u_n) \\ - \; & \left[\frac{1}{2} - \frac{1}{\pi}\arctan\left(K_U \frac{u_n + u_{max}}{u_{max}}\right)\right](u_{max} + u_n)\,, \end{aligned} \tag{7}$$

where u_n is the nominal voltage given by the underlying current controller, u_{max} is the maximum voltage which can be supplied by the power amplifier, and u_a is the actual voltage. K_U is a shaping factor. Figure 5 shows the actual voltage u_a versus nominal voltage u_n according to Equ. 7.

It is very common to limit the control current, i_c, so that the coil current i_C calculated by the main PID-controller, given by

$$i_C = i_b \mp i_c, \tag{8}$$

may vary only between zero and a maximum value. This can be modeled similar to Equ. 7 by

$$\begin{aligned} i_{C,a} = i_{C,n} \;+\; & \left[\frac{1}{2} + \frac{1}{\pi}\arctan\left(K_I \frac{i_{C,n} - i_{C,max}}{i_{C,max}}\right)\right](i_{C,max} - i_{C,n}) \\ - \; & \left[\frac{1}{2} - \frac{1}{\pi}\arctan\left(K_I \frac{i_{C,n}}{i_{C,max}}\right)\right] i_{C,n}, \end{aligned} \tag{9}$$

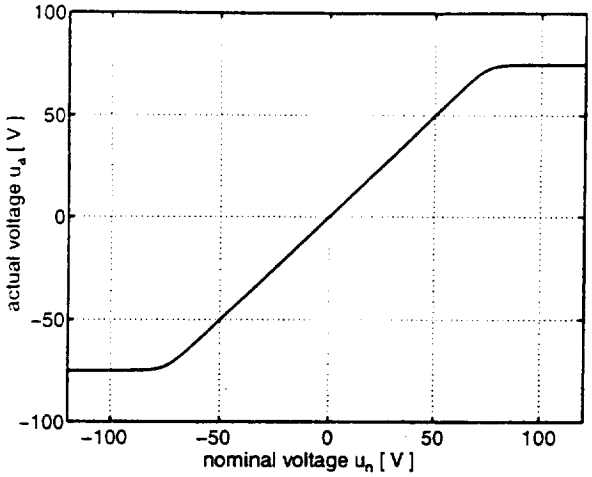

Figure 5: Actual voltage versus nominal voltage for the parameter values $u_{max} = 75.0\text{V}$ and $K_U = 10.0$.

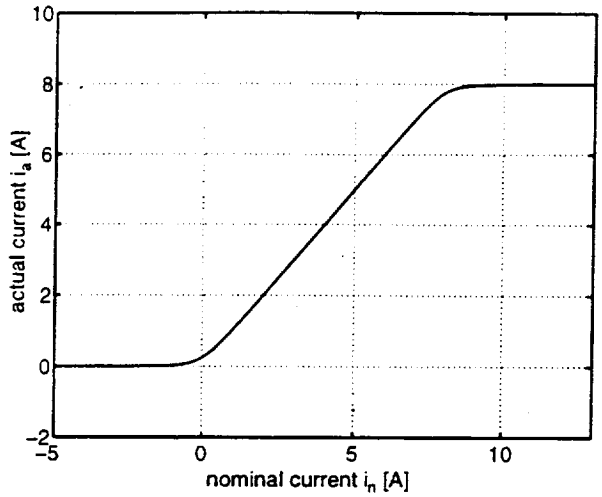

Figure 6: Actual current versus nominal current for the parameter values $i_{c,max} = 8.0\text{A}$ and $K_I = 10.0$.

where $i_{C,n}$ is the nominal coil current calculated by the main PID-controller, $i_{C,max}$ is the saturation value and $i_{C,a}$ is the actual current value at the input of the underlying current controller. K_I is a shaping factor. Figure 6 shows the actual PID-controller output $i_{C,a}$ versus the nominal current $i_{C,n}$ according to Equ. 9.

Rotor Model

The rotor is represented as a lumped mass with two degrees of freedom supported by two opposed magnetic actuators in both $x-$ and $y-$directions, see Figure 3. The rotor is excited by speed synchronous unbalance forces, which are caused by the mass imbalance eccentricity e. Thus, the equations of motion have the simple form

$$\begin{aligned} m\ddot{x} &= f_{x,mag} + me\omega^2 \cos(\omega t) \\ m\ddot{y} &= f_{y,mag} + me\omega^2 \sin(\omega t), \end{aligned} \tag{10}$$

where m is the rotor mass, $f_{x,mag}$ is the resulting magnetic force exerted on the rotor by both actuators in the $x-$direction and $f_{y,mag}$ is the resulting magnetic force exerted on the rotor by both actuators in the $y-$direction. Further, ω is the angular velocity of the rotor and t is the physical time.

Equations of Motion

A dimensionless formulation of the equations of motion can be introduced by the following dimensionless variables

$$\begin{aligned}
X &= \frac{x}{g_0} & G_{P,N} &= \frac{G_P g_0}{i_b} & L_{mi} &= \frac{\mathcal{R}_{\mathrm{mi}}}{\mathcal{R}_{\mathrm{g0}}} & U_j &= \frac{u_j}{R i_b} \\
Y &= \frac{y}{g_0} & G_{D,N} &= \frac{G_D \omega_0 g_0}{i_b} & L_{mi,0} &= \frac{\mathcal{R}_{\mathrm{mi,0}}}{\mathcal{R}_{\mathrm{g0}}} & I_j &= \frac{i_j}{i_b} \\
E &= \frac{e}{g_0} & G_{I,N} &= \frac{G_I g_0}{i_b \omega_0} & \Phi_{N,j} &= \frac{\Phi_j}{\Phi_b} & \hat{R}_N &= \frac{2 g_0 R}{k \omega_0} \\
\tau &= \frac{\omega}{2\pi} t & \Omega &= \frac{\omega}{\omega_0}, & & & &
\end{aligned} \tag{11}$$

where g_0 is the radial air gap length between the rotor and the stator at the rotor center position. The above definition of a dimensionless time τ maps one excitation period into the interval $[0, 1]$, which is useful for the formulation of the boundary value problem, see section 'Numerical Solution Methods'. $\mathcal{R}_{\mathrm{g0}}$ is the reluctance of the air gap for the center position of the rotor and $\mathcal{R}_{\mathrm{mi,0}}$ is the reluctance ofaniron path i valid for the linear range of the anhysteretic curve. They can be written as

$$\mathcal{R}_{\mathrm{g0}} = \frac{2 g_0}{\mu_0 A_g} \qquad \text{and} \qquad \mathcal{R}_{\mathrm{mi,0}} = \frac{l_{mi}}{\mu_0 \mu_{r,mi,0} A_{mi}}. \tag{12}$$

The magnetic flux is normalized by its bias value

$$\Phi_b = \frac{k i_b}{2 g_0 N \left(1 + L_{m1,0} + L_{m2,0}\right)}. \tag{13}$$

The natural frequency of the linearized system is given by

$$\omega_0 = \sqrt{k \frac{i_b^2}{m g_0^3 \left(1 + L_{m1,0} + L_{m2,0}\right)^2} \left(\frac{G_{P,I}}{1 + G_{P,I}} G_{PN} - \frac{1}{1 + L_{m1,0} + L_{m2,0}} \right)}, \tag{14}$$

and the damping ratio ζ can be written as

$$\zeta = \frac{\frac{G_{P,I}}{1+G_{P,I}} G_{DN}}{2 \left(\frac{G_{P,I}}{1+G_{P,I}} G_{PN} - \frac{1}{1+L_{m1,0}+L_{m2,0}} \right)}. \tag{15}$$

Finally, the dimensionless equations of motion have the form

$$\begin{aligned}
X'' &= \left(\frac{2\pi}{\Omega}\right)^2 \left[\frac{1 + L_{m1,0} + L_{m2,0}}{4 \left[G_{PN} \left(1 + L_{m1,0} + L_{m2,0}\right) - 1 \right]} \left(\Phi_{N,x,+}^2 - \Phi_{N,x,-}^2 \right) + E \Omega^2 \cos\left(2\pi\tau\right) \right] \\
Y'' &= \left(\frac{2\pi}{\Omega}\right)^2 \left[\frac{1 + L_{m1,0} + L_{m2,0}}{4 \left[G_{PN} \left(1 + L_{m1,0} + L_{m2,0}\right) - 1 \right]} \left(\Phi_{N,y,+}^2 - \Phi_{N,y,-}^2 \right) + E \Omega^2 \sin\left(2\pi\tau\right) \right]
\end{aligned} \tag{16}$$

and

$$\Phi'_{N,x,+} = \frac{2\pi}{\Omega} R_N \left[(1 - L_{m1,0} + L_{m2,0})\, U_{x,+,a} - \Phi_{N,x,+} (1 - X + L_{m1,x,+} + L_{m2,x,+}) \right]$$

$$\Phi'_{N,x,-} = \frac{2\pi}{\Omega} R_N \left[(1 + L_{m1,0} + L_{m2,0})\, U_{x,-,a} - \Phi_{N,x,-} (1 + X + L_{m1,x,-} + L_{m2,x,-}) \right], \tag{17}$$

where the primes denote the derivatives with respect to the dimensionless time τ, and

$$L_{mi,x,+} = L_{mi,0} \frac{\mu_{r,mi,0}}{\left[\frac{1-\mu_{r,mi,0}}{\pi} \arctan\left(K_{M,mi} \frac{|\Phi_{N,x,+}| - \Phi_{N,mi,max}}{\Phi_{N,mi,max}} \right) + \frac{1+\mu_{r,mi,0}}{2} \right]} \tag{18}$$

represents the magnetic saturation effect. The actual voltage is calculated from

$$\begin{aligned} U_{x,+,a} &= G_{P,I} \left(I_{C,x,+,a} - I_{x,+} \right) + 1 \\ &+ \left[\frac{1}{2} + \frac{1}{\pi} \arctan\left(K_U \frac{G_{P,I} \left(I_{C,x,+,a} - I_{x,+} \right) + 1 - U_{max}}{U_{max}} \right) \right] \\ &\quad \left[U_{max} - G_{P,I} \left(I_{C,x,+,a} - I_{x,+} \right) - 1 \right] \\ &- \left[\frac{1}{2} - \frac{1}{\pi} \arctan\left(K_U \frac{G_{P,I} \left(I_{C,x,+,a} - I_{x,+} \right) + 1 + U_{max}}{U_{max}} \right) \right] \\ &\quad \left[U_{max} + G_{P,I} \left(I_{C,x,+,a} - I_{x,+} \right) + 1 \right] \end{aligned} \tag{19}$$

with

$$\begin{aligned} I_{C,x,+,a} = I_{C,x,+,n} &+ \left[\frac{1}{2} + \frac{1}{\pi} \arctan\left(K_I \frac{I_{C,x,+,n} - I_{C,max}}{I_{C,max}} \right) \right] \left[I_{C,max} - I_{C,x,+,n} \right] - \\ &- \left[\frac{1}{2} - \frac{1}{\pi} \arctan\left(K_I \frac{I_{C,x,+,n}}{I_{C,max}} \right) \right] I_{C,x,+,n}. \end{aligned} \tag{20}$$

The actual coil currents are given by

$$\begin{aligned} I_{x,+} &= \frac{1 - X + L_{m1,x,+} + L_{m2,x,+}}{1 + L_{m1,0} + L_{m2,0}} \Phi_{N,x,+} \\ I_{x,-} &= \frac{1 + X + L_{m1,x,-} + L_{m2,x,-}}{1 + L_{m1,0} + L_{m2,0}} \Phi_{N,x,-}. \end{aligned} \tag{21}$$

The nominal coil currents calculated by the main PID-controller are given by

$$\begin{aligned} I_{C,x,+,n} &= 1 - G_{PN} X - G_{DN} \frac{\Omega}{2\pi} X' - G_{IN} \frac{2\pi}{\Omega} \int_0^\tau X d\tau \\ I_{C,x,-,n} &= 1 + G_{PN} X + G_{DN} \frac{\Omega}{2\pi} X' + G_{IN} \frac{2\pi}{\Omega} \int_0^\tau X d\tau. \end{aligned} \tag{22}$$

Because of the limited space only the most important equations are presented here. In order to obtain the whole set of equations the indices must be varied. In Equ. 17 to 22 the index 'x' may be substituted by 'y'. Additionally, in Equ. 18 to 20 the index '+' may be substituted by '-'.

Magnetic Force Characteristics

Defining dimesionless forces by

$$F_k = f_k \frac{g_0^2}{k i_b^2} \tag{23}$$

and considering the quasistatic case without any saturation effects the dimensionless magnetic force in $x-$direction produced by the magnet pair is given by

$$F_x = \frac{1}{4\left(1 + L_{m1,0} + L_{m2,0}\right)^2} \left(\Phi^2_{N,x,+} - \Phi^2_{N,x,-}\right), \tag{24}$$

where

$$\begin{aligned} \Phi^2_{N,x,+} &= \frac{1}{\left(1 + G_{P,I}\right)^2} \left[\frac{1 + L_{m1,0} + L_{m2,0}}{1 - X + L_{m1,0} + L_{m2,0}} \left(1 + G_{P,I}\left(1 - G_{PN}X\right)\right)\right]^2 \\ \Phi^2_{N,x,-} &= \frac{1}{\left(1 + G_{P,I}\right)^2} \left[\frac{1 + L_{m1,0} + L_{m2,0}}{1 + X + L_{m1,0} + L_{m2,0}} \left(1 + G_{P,I}\left(1 + G_{PN}X\right)\right)\right]^2. \end{aligned} \tag{25}$$

In Figure 4 the force function in $x-$direction $F_x(X)$ is plotted for various values of the proportional feedback gain G_{PN}. The effects of all saturation types presented become identical in the quasistatic case. Moreover, beyond the saturation value the resulting magnetic force is independent of the proportional feedback gain, which is plotted as a dashed line in Fig. 4.

Model Limitations

Fringing and leakage of the magnetic flux as well as magnetic flux paths, coupling different magnets, are not considered. Therefore, flux densities in different magnets are calculated from independent magnetic circuits. Any coupling between different coordinate directions is neglected. Therefore, the system is completely symmetric since no lateral static load is imposed to the shaft.

NUMERICAL SOLUTION METHODS

Nonlinear mathematical models concerning AMBs have already been investigated by several authors employing the tool of numerical simulation. However, a simulation approach, based on the Initial Value Problem (IVP) has the disadvantage that a sufficiently high number of transient cycles must be allowed to decay before a steady-state response is reached. This makes such an approach quite

cumbersome and slow, in particular near stability limits of the system. Furthermore, unstable solutions of limit cycles cannot be calculated by numerical simulation. However, a positive aspect of the simulation approach via IVP is that it is not restricted to periodic solutions and any kind of quasi-periodic or even chaotic solutions can be found.

Another widely used approach is the so-called Harmonic Balance method, which is rather an analytical than a numerical approximation. It has the advantage that both stable and unstable solutions can be obtained. However, the method does not yield stability characteristics. Since an approximation of the original system is solved, there is always the question about the validity of the results obtained.

In this investigation the numerical simulation method is an additional tool only, primarily used for verification and for calculating time response plots. It is obvious that the steady-state response of the system is basically periodic with the period T of one rotor revolution. Therefore, numerical integration is used, but formulated as a Boundary Value Problem (BVP). By employing periodic boundary conditions $z(0) = z(T)$ and solving the BVP numerically by an appropriate method any kind of stable or unstable periodic solutions can be calculated. To track solutions for a certain parameter variable, in our case the exciting unbalance frequency Ω, a smart continuation (path-following) method has to be employed. This becomes very important if so-called turning points occur during the continuation process.

The following results were obtained using the subroutine collection BIFPACK, see [Seydel, 1996]. BIFPACK provides a multiple shooting routine to solve boundary value problems, it possesses a sophisticated continuation algorithm and it can investigate the stability of a periodic solution, as outlined before. Beside other useful features the package offers a branch switching option to calculate new starting points on emanating solutions near a bifurcation.

NUMERICAL RESULTS

Solving the BVP as mentioned for the non-autonomous system with speed synchronous unbalance excitation, bifurcation diagrams can be produced with the rotor speed Ω as the chosen bifurcation parameter. Numerical simulation is used for verification and interpretation of the obtained stable or unstable periodic solutions.

In the following, system responses are discussed for certain parameter values in order to show the most interesting results of this research. Since a fully symmetrical problem is discussed, all diagrams are valid for both $x-$ and $y-$direction. Figure 7 shows the steady-state amplitudes of the rotor vibration in $x-$ and $y-$direction, respectively, versus the dimensionless excitation frequency Ω. Stable periodic solutions are represented by solid lines, unstable periodic solutions by dashed lines. All presented solutions are calculated for the parameter values $G_{PN} = 3.0$, $G_{DN} = 1.34$, $I_{C,max} = 2.0$, and $E = 0.35$.

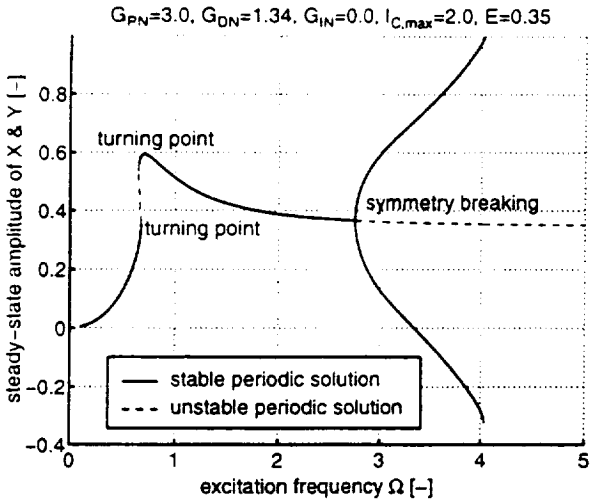

Figure 7: AMB System response without integral feedback gain.

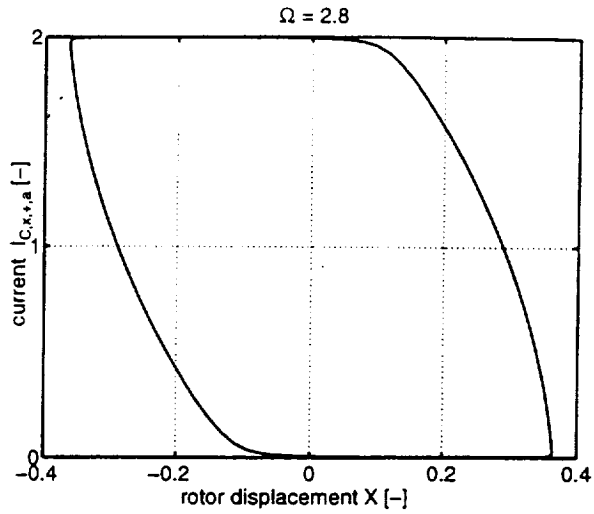

Figure 8: Saturation effect of the output of the main PID-controller in the neighborhood of the bifurcation point.

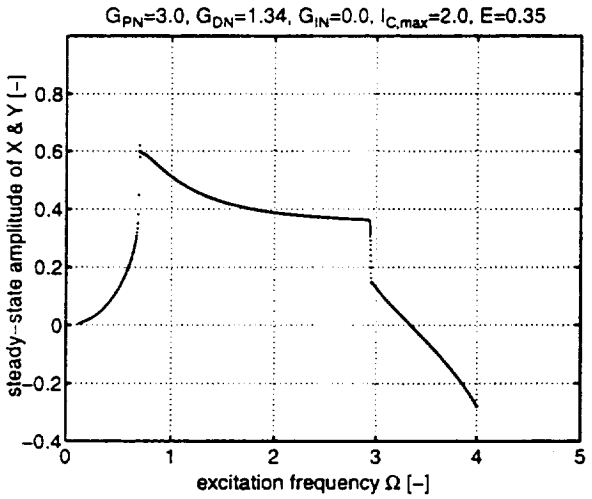

Figure 9: Numerical simulation results with stable lower unsymmetric branch.

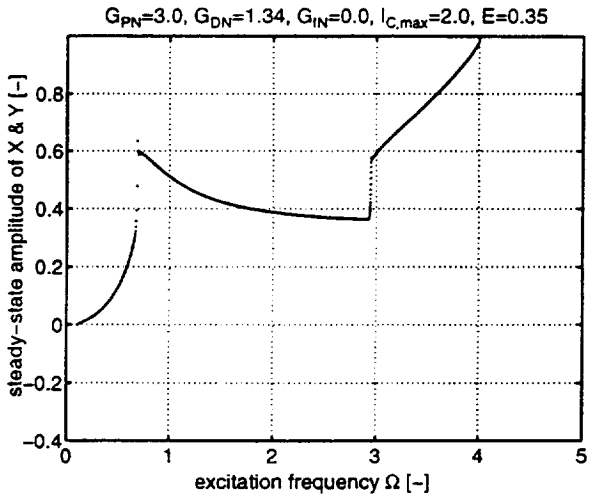

Figure 10: Numerical simulation results with stable upper unsymmetric branch.

The system response without integral feedback is shown in Fig. 7. Sweeping from low to high values of the excitation frequency, at $\Omega = 0.67$ a turning point occurs. Because of the softening spring characteristic of the system the resonant curve bends to the left until a second turning point at $\Omega = 0.64$ is reached. For all frequency values between these two turning points three coexisting periodic solutions exist, i.e. two stable solutions and one unstable solution. This causes jump and hysteresis phenomena when changing the excitation frequency across this region.

Increasing the frequency far beyond the eigenfrequency of the linearized system at $\Omega = 1.0$, another nonlinear phenomenon occurs. At $\Omega = 2.75$ symmetry breaking is detected. At this

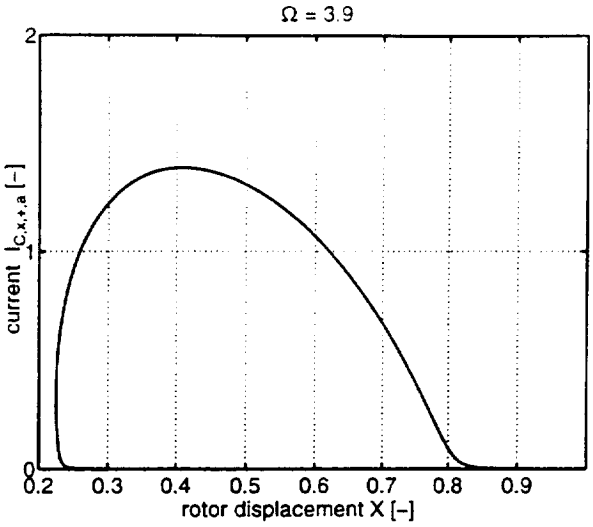

Figure 11: Output of PID-controller for electromagnet 'x,+' (on upper stable branch).

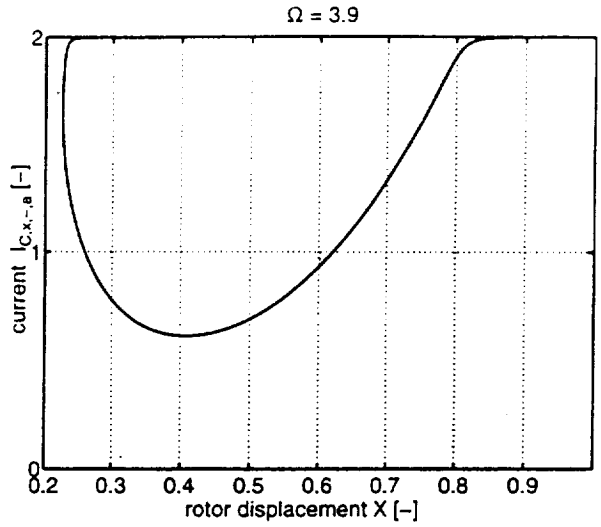

Figure 12: Output of PID-controller for electromagnet 'x,-' (on upper stable branch).

bifurcation point the symmetric periodic solution becomes unstable, when a stable unsymmetric solution emanates. The maximum and minimum values of the rotor vibrations are not equal in the case of an unsymmetric solution. However, four different stable rotor orbits are possible which are symmetric with respect to the $x-$ or $y-$axis, respectively.

At $\Omega = 4.03$ the system response curve of both stable unsymmetric periodic solutions ends, because of contact between the rotor and the stator. However, the contact problem is beyond the scope of this work. Concerning the motion of a rotor with contact different types of bifurcations and nonlinear phenomena are discussed in [Ecker, 1997] and [Ecker, 1998], for example.

Note, that in Fig. 7 and subsequent diagrams rotor motion is considered only in one axis of the AMB. Therefore, maximum amplitudes at contact of $X_{max} = X_{cont} = 1.0$ are possible. In the case that both axes are considered maximum amplitudes in $x-$ and $y-$direction at contact are limited according to $\sqrt{X_{cont}^2 + Y_{cont}^2} = R_{max} = 1.0$. In Fig. 7 this situation occurs at $\Omega = 3.63$.

The frequency value of the bifurcation point depends on the differential feedback gain. It can be shifted to lower frequencies by increasing the differential feedback gain G_{DN}. Symmetry breaking is caused by saturation of the nominal coil current required by the main PID-controller, see Fig. 8, 11 and 12.

In order to verify the results obtained by BIFPACK. additional numerical simulations are carried out. By slowly increasing the excitation frequency from $\Omega = 0.0$ to $\Omega = 4.0$ identical results are obtained, see Fig. 9 and 10. Each point of the plotted curve represents the maximum of rotor displacement during one period of unbalance excitation. Therefore, the transient behaviour of the jump phenomenon can be seen in Fig. 9 and 10. It depends on the initial conditions, which stable unsymmetric branch is picked by the system. Practically speaking the branches are randomly chosen

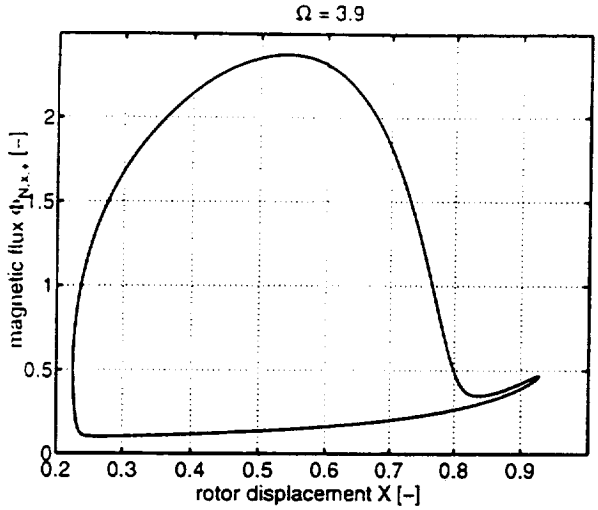

Figure 13: Magnetic flux for electromagnet 'x.+' (on upper stable branch).

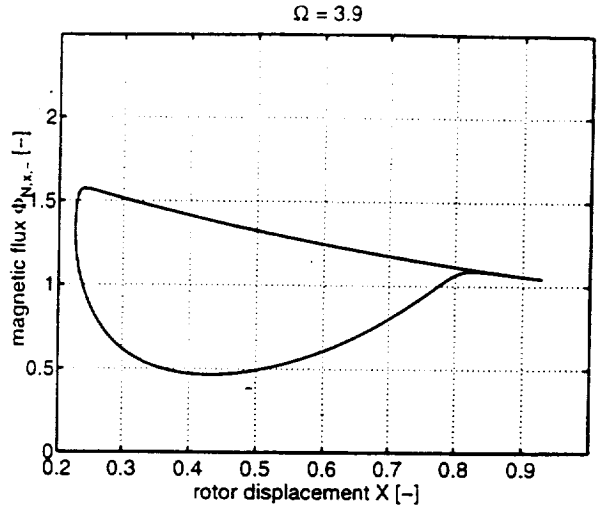

Figure 14: Magnetic flux for electromagnet 'x,-' (on upper stable branch).

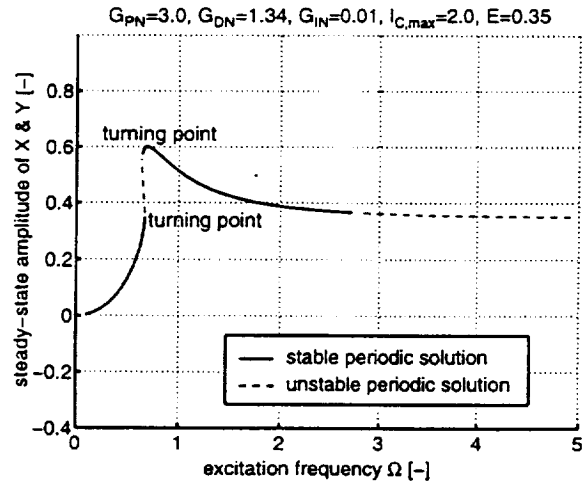

Figure 15: AMB system response with integral feedback gain.

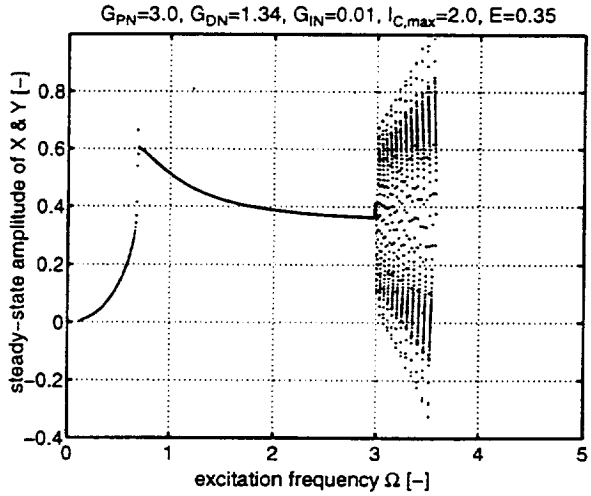

Figure 16: Numerical simulation results with integral feedback gain.

corresponding to arbitrary initial conditions.

Figure 11 and 12 show the coil currents calculated by the main PID-controller for the upper stable branch at $\Omega = 3.9$. The plots show a strong nonlinear characteristic caused by saturation. The magnetic flux for the same parameter set is plotted in Fig. 13 and 14 respectively.

For all results presented only the output of the PID-controller exceeds the saturation value. Both the voltage of the power amplifier and the magnetic flux density remain well within the linear range.

Turning on the integral feedback gain G_{IN} stable periodic branches could not be found anymore

beyond the speed threshold of $\Omega = 2.75$, see Fig. 15. Instead, a quasiperiodic motion of the rotor occurs, which is detected by numerical simulation results, see Fig. 16. Because of symmetry breaking the integral part of the control current constantly increases the output of the PID-controller. Beyond the saturation value the influence of the proportional and differential feedback decreases almost down to zero-value. This would be changed by introducing a separate saturation level only for the integral part of the control current well below the saturation value for the whole output of the PID-controller.

CONCLUSION

AMB systems show important nonlinear phenomena if nonlinear components are included in the analysis. This investigation discusses vibration effects of saturation of the PID-controller output. Numerical results obtained by solving a boundary value problem combined with the path following method are presented. Stable and unstable periodic solutions are calculated. For specific parameter sets symmetry breaking and quasiperiodic solutions may occur. It is shown that important phenomena exist in AMB systems which are not predictable by linear methods. Future investigations will be carried out to discuss further interesting parameter sets. Higher sophisticated models including more components, as for example geometric coupling and static preload, will be investigated.

ACKNOWLEDGEMENT

The authors gratefully acknowledge the support of this project by the Austrian science foundation 'Fonds zur Förderung der wissenschaftlichen Forschung (FWF)'.

REFERENCES

[Chinta, et al., 1996] Chinta, M., Palazzolo, A.B., Kascak, A., *Quasiperiodic Vibration of a Rotor in a Magnetic Bearing with Geometric Coupling*, Proc. of 5th Int. Symp. on Magnetic Bearings, Kanazawa, Japan, 1996.

[Ecker, 1998] Ecker, H., *Nonlinear stability analysis of rigid single mass rotor contacting a rigid auxiliary bearing*, IFToMM Proc. of Fifth Int. Conf. on Rotor Dynamics, (Irretier,H., Nordmann,R.,ed.), pp. 790-801, Darmstadt, Germany, Sept. 7-10, 1998.

[Ecker, 1997] Ecker, H., *Steady-state orbits of an AMB-supported rotor contacting the backup bearings*, Proc. of Indust. Conf. of Magnetic Bearings MAG'97, (Allaire,P.,ed.), pp. 129-138, Alexandria, VA, Aug. 21-22, 1997.

[Ecker, et al., 1997] Ecker. H., Knight, J.D., Wu, L., *Nonlinear Dynamic Simulation of an Active Magnetic Bearing System with Non-symmetric Coordinate Coupling Forces*, Proc. of Int. Gas

Turbine & Aeroengine Congress & Exhibition, Orlando, Florida, ASME Conf. paper No. 97-GT-113, 1997.

[Haferl, Springer, 1991] Haferl, A., Springer, H., *Simulation von Magnetisierungsprozessen in Magnetlagern*, Proc. of 7. Symp. Simulationstechnik, ASVM-Tagung in Hagen, Verlag Vieweg, 1991.

[Hebbale, 1985] Hebbale, K.V., *A Theoretical Model for the Study of Nonlinear Dynamics of Magnetic Bearings*, Ph.D. thesis, Cornell University, 1985.

[Hebbale, Taylor, 1986] Hebbale, K.V., Taylor, D.L., *Nonlinear Dynamics of Attractive Magnetic Bearings*, Proc. of the Workshop on Rotordynamic Instability Problems in High-Performance Turbomachinery, Texas A&M-Univ., NASA-Conf. Publ. No. 2443, 1986.

[Hoffmann, et al., 1997] Hoffmann, K.-J., Laier, D., Markert, R., *Nonlinear Control of Magnetically Supported Rotors*, Proc. of MAG'97 - Industrial Conference and Exhibition on Magnetic Bearings, Alexandria, VA, 1997.

[Jeong, et al., 1994] Jeong, H.S., Kim, C.S., Lee, C.W., *Modelling and Control of Cone Shaped Active Magnetic Bearing Systems*, Proc. of 4th Int. Symp. on Magnetic Bearings, ETH-Zürich, 1994.

[Knight, Ecker, 1996] Knight, J.D., Ecker, H., *Simulation of Nonlinear Dynamics in Magnetic Bearings with Coordinate Coupling*, Proc. of Summer Computer Simulation Conf., Portland, Oregon, 1996.

[Knight, et al., 1993] Knight, J., Walsh, T., Virgin L., *Dynamic Analysis of a Magnetic Bearing System with Flux Control*, Proc. of 2nd Int. Symp. on Magnetic Suspension Technology, Seattle, WA, 1993.

[Knight, et al., 1992] Knight, J.D., Xia, Z., McCaul, E.B., *Forces in Magnetic Journal Bearings: Nonlinear Computation and Experimental Measurement*, Proc. of 3rd Int. Symp. on Magnetic Bearings, Alexandria, VA, 1992.

[Lang, et al., 1995] Lang, O., Wassermann, J., Springer, H., *Adaptive Vibration Control of a Rigid Rotor supported by Active Magnetic Bearings*, Proc. of Int. Gas Turbine and Aeroengine Congress and Exposition, Houston, Texas, 1995.

[Mohamed, Emad, 1993] Mohamed, A.M., Emad, F.P., *Nonlinear Oscillations in Magnetic Bearing Systems*, IEEE Transactions on Automatic Control, Vol. 38, No.8, 1993.

[Moser, 1993] Moser, F., *Stabilität und Verzweigungsverhalten eines nichtlinearen Rotor-Lager-Systems*, Ph.D. thesis, Vienna University of Technology, 1993.

[Nataraj, 1995] Nataraj, C., *Nonlinear Analysis of a Rigid Rotor on Magnetic Bearings*, Proc. of Int. Gas Turbine and Aeroengine Congress and Exposition, Houston, ASME Conf. paper No. 95-GT-204, 1995.

[Satoh, et al., 1990] Satoh. I., Murakama, C., Nakajima, A., Kanemitsu, Y., *A Self-Excited Vibration of Magnetic Bearing Systems with Flexible Structure*, Proc. of 2nd Int. Symp. on Magnetic Bearings, Tokyo, 1990.

[Schweitzer, et al., 1993] Schweitzer, G., Traxler, A., Bleuler, H., *Magnetlager, Grundlagen, Eigenschaften und Anwendungen berührungsfreier, elektromagnetischer Lager*, Springer Verlag, Berlin, 1993.

[Seydel, 1996] Seydel R., *BifPack, a Program Package for Continuation, Bifurcation and Stability Analysis*, Program documentation, University of Ulm, Germany, 1996.

[Sinha, 1990] Sinha, A., *On the Design of Magnetic Suspension Systems*, Proc. of Gas Turbine and Aeroengine Congress and Exposition, Belgium, ASME Conf. paper No. 90-GT-239, 1990.

[Springer, et al., 1990] Springer, H., Maslen, E.H., Humphris, R.H., *Nonlinear Hysteresis Effects in Electromagnetic Bearings*, Proc. of 3rd Int. Conf. on Rotordynamics, Lyon, (Ed.du CNRS), 1990.

[Springer, et al., 1998] Springer, H., Schlager, G., Platter T., *A Nonlinear Simulation Model for Active Magnetic Bearing Actuators*, Proc. of 6th Int. Symp. on Magnetic Bearings, MIT Cambridge, MA, 1998.

[Steinschaden, Springer, 1999] Steinschaden, N., Springer, H., *Some Nonlinear Effects of Magnetic Bearings*, Proc. of the 1999 ASME Design Engineering Technical Conferences, Las Vegas, Nevada, ASME Conf. paper No. DETC99/VIB-8063, 1999.

[Troger, Steindl, 1991] Troger, H., Steindl, A., *Nonlinear Stability and Bifurcation Theory*, Springer Verlag, Wien - New York, 1991.

[Virgin, et al., 1994] Virgin, L., Walsh, T.F., Knight, J.D., *Nonlinear Behavior of a Magnetic Bearing System*, Proc. of Int. Gas Turbine and Aeroengine Congress and Exposition, The Hague, Netherlands, ASME Conf. paper No. 94-GT-341, 1994.

[Wang, et al., 1994] Wang, H., Wu, Z., Niu, X., *Dynamic Bifurcations of Active Magnetic Bearings Rotor Systems*, Proc. of 4th Int. Symp. on Magnetic Bearings, ETH-Zürich, 1994.